Title

Experimental and Computational Development of a Conformationally Flexible Template for the meta-C-H Functionalization of Benzoic Acids.

Journal

Journal of the American Chemical Society, 139(31)

Authors

Fang, Lizhen
Saint-Denis, Tyler
Taylor, Buck
et al.

Publication Date

2017-08-09

DOI

10.1021/jacs.7b03296

Peer reviewed

HHS Public Access

Author manuscript

J Am Chem Soc. Author manuscript; available in PMC 2024 May 11.

Published in final edited form as:

J Am Chem Soc. 2017 August 09; 139(31): 10702–10714. doi:10.1021/jacs.7b03296.

Experimental and Computational Development of a Conformationally Flexible Template for the *meta*-C–H Functionalization of Benzoic Acids

Lizhen Fang[†,‡,‖], **Tyler G. Saint-Denis**[†,‖], **Buck L. H. Taylor**[§,‖], **Seth Ahlquist**[§], **Kai Hong**[†], **SaiSai Liu**[‡], **LiLi Han**[‡], **K. N. Houk**[*,§], **Jin-Quan Yu**[*,†]

[†]The Scripps Research Institute, 10550 North Torrey Pines Road, La Jolla, California 92037, United States

[‡]School of Pharmacy, Xinxiang Medical University, Xinxiang Shi, Henan Province 453003, People's Republic of China

[§]Department of Chemistry and Biochemistry, The University of California, Los Angeles, California 90095, United States

Abstract

A conformationally flexible template for the *meta*-C–H olefination of benzoic acids was designed through both experimental and computational efforts. The newly designed template favors a silver–palladium heterodimer low barrier transition state, and demonstrates that it is feasible to lengthen templates so as to achieve *meta*-selectivity when the distance between the functional handle of the native substrate and target C–H bond decreases. Analysis of the *ortho*-, *meta*-, and *para*-C–H cleavage transition states determined that the new template conformation optimizes the interaction between the nitrile and palladium–silver dimer in the *meta*-transition state, enabling palladium to cleave *meta*-C–H bonds with moderate-to-good yields and generally high regioselectivity. Regioselectivity is governed exclusively by the template, and kinetic experiments reveal that there is a 4-fold increase in rate in the presence of monoprotected amino acid ligands. Using a Boltzmann distribution of all accessible C–H activation transition states, it is possible to computationally predict *meta*-selectivity in a number of investigated templates with reasonable accuracy. Structural and distortion energies reported may be used for the further development of templates for *meta*-C–H activation of hitherto unexplored arene substrates.

Graphical Abstract

[*]**Corresponding Authors**: houk@chem.ucla.edu, yu200@scripps.edu.

[‖]L.F., T.G.S.-D., and B.L.H.T. contributed equally.

Supporting Information

The Supporting Information is available free of charge on the ACS Publications website at DOI: 10.1021/jacs.7b03296.

Synthesis of compounds, characterization data, and computational details (PDF)

The authors declare no competing financial interest.

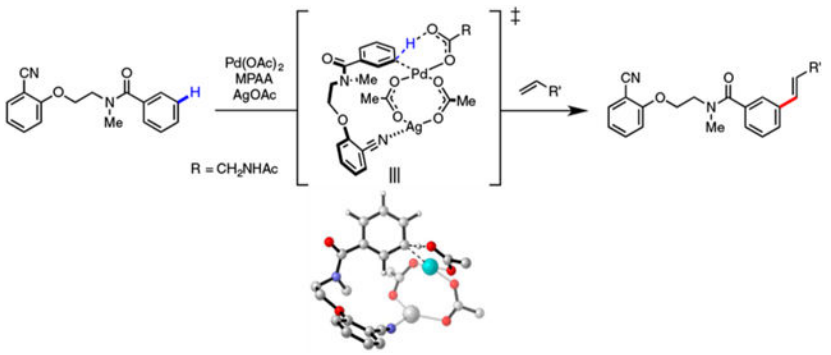

1. INTRODUCTION

Transition-metal-catalyzed C–H activation has been extensively studied due to its potential to directly convert C–H bonds into C–C as well as C–heteroatom bonds, and in so doing expedite synthetic endeavors and reduce waste and cost traditionally associated with organic synthesis.[1] The ubiquity of C–H bonds in organic substrates offers a myriad of opportunities to modify molecular structure through transition-metal-catalyzed C–H activation; however, such opportunities depend on the development of strategies to precisely control site-selectivity during C–H activation. Because steric and electronic properties of multiple C–H bonds in a given molecule are similar, the recognition of distal and geometric relationships of a target C–H bond with respect to a functional group has afforded a powerful means of achieving site selectivity.[2] While the use of practical directing groups has allowed synthetic chemists to achieve functionalization of C–H bonds that are proximate and accessible in terms of geometry,[3] those C–H bonds that are six bonds away from a directing group or geometrically inaccessible are difficult to functionalize in a controllable manner.

To fully exploit the power of this approach, it is necessary to systematically design templates to match different classes of substrates and C–H bonds located at various positions.[4] In this context, we have recently developed several U-shaped end-on nitrile templates that can direct palladation of remote *meta*-C– H bonds[5] by accommodating a highly strained cyclophane-like transition states. Our group and others have also developed various templates to extend to other substrate classes such as hydrocinnamic acids, phenyl acetic acids, and benzyl alcohols/amines (Figure 1a).[6] In almost all previous reports of template-mediated *meta*-C–H activation, the template is an inherently rigid amide structure connecting to a coordinating nitrile or pyridine,[7] whereas the native substrate contains a conformationally flexible alkyl chain. Further, the distance from the target C–H bond and the functional handle (e.g., an acid, amide) of the substrate is typically 5–6 atoms (Figure 1a), and the distance between the target C–H bond and the installed nitrile-coordinating moiety is typically 10–11 atoms (Figure 1a). Herein, we report the development of a simple template that enables the *meta*-olefination of benzoic acids, typified by the following: (A) a distance from target C–H bond and functional handle of 4 atoms (Figure 1b); (B) a distance from target C–H bond to template nitrile of 12 atoms (Figure 1b); and (C) a template containing a conformationally flexible alkyl chain wherein conformational flexibility is

imparted by the template rather than the substrate. That is to say, when the distance from the functional handle and the target C–H bond is shortened from 6 or 5 bonds (hydrocinnamic acid and phenylacetic acid substrates, respectively) to 4 atoms (benzoic acids), we are able to compensate by lengthening the net distance of the template nitrile to the target C–H bond and in so doing achieve the same cyclophane transition state (Figure 1b).[8] Strain energies of simple cyclophanes range from about 30 kcal/mol for [2.2]-paracyclophane to about 2 kcal/mol for [4.4]-paracyclophane and larger;[9] the distortion/strain energy of successful templates in this study is in the same range as those of large cyclophanes (1–2 kcal/mol). Our experimental efforts and template design were guided by computational studies, and the mechanism for this novel template's high regioselectivity was evaluated by both computational as well as kinetic studies.

Several computational studies have been performed to elucidate the mechanism of nitrile-enabled *meta*-C–H activation, and two distinct pathways have been elucidated: Houk and Wu[10] have used density functional theory to elucidate the mechanism and origins of *meta*-regioselectivity in our Pd(II)-catalyzed C–H olefinations of benzylic ethers as well as hydrocinnamic acids employing the aforementioned nitrile templates (Figure 1a). In the *meta*-selective C–H activation of hydrocinnamic acid derivatives,[10a] it was determined that the monoprotected amino acid (MPAA) ligands act as both a dianionic bidentate ligand and a proton acceptor; in other words, the MPAA ligand serves dual roles in the (A) stabilization of monomeric Pd complexes and (B) the intramolecular deprotonation of the arene substrate in the concerted metalation-deprotonation (CMD) C–H cleavage transition state. Conversely, in the *meta*-C–H activation of benzylic ethers study,[10b] a completely different mechanism was observed so as to rationalize our observation that no ligand is needed for high yields and high *meta*-selectivity: although the C–H activation step also proceeds by a concerted CMD pathway and this is both rate- and regioselectivity-determining, the lowest accessible transition state contains a heterodimeric Pd-(μ-OAc)$_3$Ag species in which the nitrile group coordinates the Ag, which bridges the Pd by two acetates, placing Pd adjacent to the *meta*-C–H bond, explaining the high regioselectivity. This previous study unveiled the importance of distortional energy of the template on the C–H activation step and has shed some light on the necessary requirements for *meta*-selectivity. Specifically, it was determined that in the *meta*-C–H activation of benzylic ethers, bulky *i*-Bu and *t*-Bu substituents at specific locations on the template were critical for reactivity as well as *meta*-selectivity by enabling predistortion of the template into a transition state-like conformation.

Armed with the aforementioned experimental insights and computational insights, we endeavored to use computational methods for the rational design of a nitrile template for *meta*-C–H olefination of benzoic acid substrates and evaluate the scope of both benzoic acid derivatives as well as olefin coupling partners using said template (Figure 1b). Compared to the extensive development of *ortho*-functionalization of benzoic acids,[11] *meta*-C–H olefination of benzoic acids remains an unsolved challenge, with scarce examples appearing in the literature.[12] We previously investigated a nondirected Pd(II)-catalyzed olefination (Fujiwara–Moritani reaction) of electron-deficient arenes including benzoic esters[13] as well as a nondirected rhodium(II) olefination of benzoic esters, although the former reaction requires the arene substrate to be used as solvent and the latter reaction gave poor regioselectivity and poor yields.[14] Several other reports exist for the *meta*-olefination of

benzoic esters in the absence of directing groups,[14,15] although these reactions suffer from either poor regioselectivity or require blocking at the *para*-position. To date, no efficient, practical, and directed regioselective method exists for the *meta*-olefination of benzoic acids. From the perspective of synthetic applications, said reaction would be appealing given the dearth of methodology for the production of cinnamic acid derivatives as well as vinylarenes with carboxyl groups at the *meta*-position; this motif appears in several compounds of pharmacological interest such as carboline derivative **1a**[16] and octahydrophenanthrene derivative **1b**,[17] which are inhibitors of cGMP-specific phosphodiesterases and modulators of gluticosteroid receptors, respectively (Figure 1c).

This study reports the logical design, experimental investigation, and computational evaluation of a surprisingly flexible 2-(2-(methylamino)ethoxy)benzonitrile template (Figure 1b), which lacks the steric bulk characteristic of our previously reported templates for *meta*-C–H activation. This template is capable of effecting generally good C–H activation with yields up to 98% and *meta*-regioselectivity up to 92%. Computationally, we propose that the nitrile on the designed template coordinates Ag, rather than Pd, and that mechanistically this *meta*-olefination occurs through a Pd-(μ-OAc)$_3$-Ag heterobimetallic intermediate in which Pd is precisely poised to activate the target *meta*-C–H bond. This information builds upon our previous works and will likely alter the future design of templates for C–H activation by shedding light on the possibility of metallic dimers involved in the key C–H cleavage step of these reactions.

2. RESULTS AND DISCUSSION

2.1. Reaction Optimization.

We began our investigations into the *meta*-olefination of benzoic acids by screening template adducts T_1–T_4 (Table 1), all of which are typified by a target *meta*-C–H bond being 12 atoms away from the nitrile moiety, for olefination with ethyl acrylate in the presence of Ac-Gly-OH in the presence of silver as a terminal oxidant. T_1 and T_2 represent more rigid template frameworks, whereas T_3 and T_4 represent more flexible template structures. T_1 provided the corresponding olefination products in 76% yield with 88% *meta*-selectivity and a mono olefination/diolefination (mono:-di) ratio of 5:1, while T_2 had a lower yield of 43%, but exhibited improved *meta*-selectivity (95%) and an improved mono:di ratio. Remarkably, T_3 was olefinated in 98% yield, with 91% *meta*-selectivity and a mono:di ratio of 10:1, while T_4 exhibited depreciated reactivity and selectivity. These findings are intriguing, given that from the outset it was expected that rigid frameworks (T_1, especially T_2, which possesses geminal dimethyl groups and by the Thorpe–Ingold effect should favor cyclization) would encourage formation of the necessary cyclophane for remote Pd-catalyzed C–H cleavage. Consequently, several control templates were subsequently designed to further attempt to highlight the remarkable reactivity and regioselectivity of T_3. First, T_5 lacking the nitrile template possessed little *meta*-selectivity and low reactivity, underscoring the intrinsic electronic preferences for Pd-catalyzed olefination. Second, T_6 was designed and tested under the pretense that the presence of the *N*-methyl was paramount for cyclophane formation; the reduced yield and selectivity obtained with substitution with isopropyl lends some support to this hypothesis.

Two other templates, T_7 and T_8, were evaluated, both of which contained geminal dimethyl groups α to the amide, and the latter contained the *N*-methyl present in T_3; these both exhibited poorer yields and reduced selectivities. It is worth noting that T_7 exhibited *meta*-selectivity close to that of T_5 (i.e., inverted selectivity), such that comparison in the regioselectivity preferences of T_7 and T_5 underscores the necessity of methyl-substitution on the amide nitrogen. Finally, the homologated template T_9 was observed to have drastically depreciated yield as compared to T_3 (i.e., 16%) with only slight preference for *meta*-olefination. Subsequently, we sought to understand the influence of temperature, AgOAc, ligand, as well as $Pd(OAc)_2$ loadings on the reaction of **2a** containing T_3 (Table 2). It is evident that removal of Ac-Gly-OH (entry 2) dramatically reduces yields; that said, it is worth noting that the selectivity still favors *meta*-olefination. Removal of AgOAc and only allowing air to serve as the terminal oxidant only cuts the yield in slightly more than one-half (entry 3), and decreasing $Pd(OAc)_2$ loadings to 5 mol % only slightly reduces the yield (entry 4). This outcome of the reaction is sensitively dependent on temperature (entries 5–8), but selectivity is largely unaffected.

We next sought to evaluate the scope of this template-assisted *meta*-olefination in other substrate classes. Although the initially disclosed conditions (e.g., use of Ac-Gly-OH) gave high yields and selectivities in the simple benzoic acid derivative, this method was not found to be broadly applicable to other benzoic acid derivatives such as **2b** (entry 1). We believe that the steric repulsion imparted by *ortho*-substitution clashes with the requisite amide bond of our benzoic acid substrates, thus resulting in an initially lower-yielding reaction. However, we endeavored to screen other monoprotected amino acids and bases, and in so doing we believed we could optimize conditions to afford a more reactive catalyst, therefore resulting in superior yields and higher selectivities for *ortho*-substituted substrates. Consequently, we pursued further development of conditions that are potentially compatible with a broad range of benzoic acids (Table 3). The addition of various bases (entries 2–9) only hampered the reaction, and switching to bulkier ligands (entries 10–16) diminished reactivity almost entirely. Screening simple acetyl-protected amino acids led to improved reactivity (entries 17–23), while acid (entries 21 and 22) decreased the yield (compare to entry 20), and addition of sodium tosylate (entry 23) slightly increased the yield, improved *meta*-selectivity, and provided a larger mono/di ratio. With improved conditions in hand, we proceeded to investigate the breadth of this reaction on various substituted benzoic acid substrates (Table 4).

The parent benzoic acid (**2a**) provides both mono- and disubstituted adducts. Benzoic acids with substitution at the *ortho* position react in good yields when the *ortho* substitution is electron-donating (**3b**, **3c**), and when *ortho*-substitution is electron-withdrawing (**3d**) the yield is diminished but selectivity still favors *meta*-substitution. Substitution at the *meta*-position (*m′*) led to decreased yields when electron-donating groups were present as well as diminished selectivity (**3e**, **3f**), which can be explained by electronic biases (e.g., the methoxy group in **3f** formally directs electron density to the *ortho*-position). *meta′*-Substitution with fluorine (**3g**) decreased yield and decreased selectivity, yet *meta′*-substitution with chlorine decreased yield but still led to high *meta*-selectivity (**3h**).

para-Substitution with electron-poor and electron-donating groups (**3i** and **3j**, respectively) generally gave good yields and high selectivity. The moderate yield of **3i** is likely due to the steric bulk imparted by methoxy substitution. Finally, disubstitution at the *ortho*- and *ortho′* -positions (**3k**) as well as the *ortho′* - and *meta′* - (**3l** and **3m**) and the *meta′* - and *para*-positions (**3n**) all gave moderate-to-good yields as well as high *meta*-selectivity. The scope of olefin coupling partners was also briefly examined (Table 5). Olefins including *α,β*-unsaturated ketones, aldehydes, alkyl and benzylic esters, amides, as well as phosphonates were all competent olefins (**4a**–**4f**). Unfortunately, and consistent with past findings, simple alkyl olefins are unreactive. Further, although products **4e** and **4f** were produced in lower yields, high *meta*-selectivity was still observed. It is worth noting that the template is also easily removable (see the Supporting Information).

2.2. Computational Elucidation of *meta*-Selectivity.

Given the lack of geminal disubstitution or rigidity in T_3, it was imagined from the outset that this template would be relatively flexible as compared to other investigated templates. Such flexibility, due to the presence of two contiguous methylene carbons as well as a phenolic ether oxygen, would presumably result in enhanced degrees of freedom of conformational states through rotation, and thus diminish selectivity. Indeed, increasing the number of methylene carbons in templates, such as is the case of the homologous template T_9, dramatically decreases yield as well as *meta*-selectivity.

Perplexed by the reactivity and, more importantly, selectivity of the simplest template investigated, T_3, we investigated these reactions computationally. We began by first identifying possible transition states of the C–H cleavage of the simple benzoic acid with T_3 (Table 6) and determining their preferences for *ortho*-, *meta*-, as well as *para*-selectivity. Initially, we expected that the active catalyst would be monomeric palladium ligated by a dianionic *N*-acetylglycine ligand (Pd–Gly), because reaction conditions are similar to our previous studies[10a] and because removal of ligand dramatically decreases the yield of the reaction, as stated earlier. That said, calculations indicate that the *para*-olefination adduct should be favored under this mechanism with a barrier of 24.7 kcal/mol for *para*-C–H cleavage, while *meta*-C–H cleavage has a barrier of 26.1 kcal/mol. Consequently, we sought to evaluate other possible transition states, including a palladium–silver heterodimer, a palladium–palladium dimer in the absence of a ligated *N*-acetyl–glycine (Pd–Ag and Pd–Pd, respectively), as well as a transition state characterized by monomeric palladium in the absence of *N*-acetyl–glycine (Pd). Intriguingly, *meta*-selective C–H activation for the Pd–Ag transition state had the lowest barrier (23.2 kcal/mol) as compared to all other transition states evaluated. The *meta*-olefination product is also favored by the palladium homodimer mechanism, Pd–Pd, but this is higher in energy as compared to the Pd–Ag mechanism.

Theoretical regioselectivities were next computed using a Boltzmann distribution of all low-energy transition-state conformations. Because of the flexible nature of the template, a large number of conformations were located for each transition state, many of which were within 3 kcal/mol of the global minimum, thus contributing to product formation. When the favored Pd–Ag mechanism is considered in isolation, it is predicted that the transition state favors *meta*-selectivity by 98%, an overestimation as compared to the experimentally observed

meta-olefination of T_3 (91%). However, because the monomeric Pd–Gly mechanism is only 1.5 kcal/mol higher in energy, some of the minor regioisomers could result from the Pd–Gly mechanism. When low-energy conformations for both mechanisms are factored into the Boltzmann distribution, the computationally predicted regioselectivity drops to 94% *meta*-selective C–H activation, which is in excellent agreement with the experimental observations of 91%. It is important to note that there will be significantly greater error in comparing the free energies of monomeric, dimeric, and heterodimeric transition states (perhaps 2–3 kcal/mol),[18] than comparing regioisomeric transition states of one type, such that the agreement may be in part serendipitous. Nevertheless, the calculations suggest a delicate balance between monomeric and heterodimeric mechanisms.

We next sought to understand the *meta*-selectivity for the Pd–Ag mechanism in greater detail. The lowest energy conformation of T_3 places the amide and aryloxy groups in a gauche-type conformation (Figure 2). This geometry is maintained in the *meta*-transition state, Pd–Ag, resulting in a low template distortion energy ($\Delta E^{\ddagger}_{\text{template distortion}}$) of 1.4 kcal/mol. This is the energy required to distort the template into the transition-state geometry without distorting the target C–H bond. In contrast, greater conformational changes are necessary in the *ortho*- and *para*-transition states, with distortion energies of 3.3 and 4.8 kcal/mol, respectively. The interaction between the catalyst and the template is also strongest in the *meta*-transition state, because this template conformation allows the optimal interaction between the nitrile and the silver atom.[19]

Because structural factors are clearly paramount in the regioselectivity imparted by templates, several templates we evaluated experimentally in Table 1 were subsequently studied with computation to gain insight into the specific structural features that favor *meta*-selectivity. In particular, we sought to understand why the homologated template T_9 and the ester template T_4 afforded product distributions with decreased *meta*-selectivity. Adopting the analysis used in Table 6, both Pd–Gly and Pd–Ag mechanisms were modeled for each template of interest, and selectivities were computed using the aforementioned Boltzmann distribution analysis. Interestingly, our calculations show that the computed selectivity of the Pd–Gly monomer pathway varies drastically depending on the template structure (see entries 1–7, Table 7). The disagreement of these computed selectivity with our experimental observations suggests that the Pd–Gly monomer is unlikely to be operative. Remarkably, when the Pd–Ag mechanism is modeled for each template, *meta*-selectivity is consistently favored, particularly for the most selective template (entries 1–4), lending additional support for this mechanism.

While the heterodimer mechanism Pd–Ag predicts the correct regioisomer, the level of selectivity is typically overestimated. This is especially problematic for poorer templates, such as T_4 and T_9 (entries 5 and 6, respectively): experimentally T_4 gives a low *meta*:others regioselectivity of 47:53 (negligible regioselectivity), but the regioselectivity predicted by the Pd–Ag mechanism is 85% *meta*-product; T_9 gives a *meta*:others regioselectivity of 63:37, but the predicted regioselectivity is 71% *meta*-product. Despite these seemingly incongruent predictions, when the same Boltzmann distribution analysis of all conformations of the two competing transition states Pd–Gly and Pd–Ag is taken into

account in computational prediction, it is possible to make fairly accurate predictions on *meta*-selectivity.

This appears to be especially true for templates T_4 and T_9, in which the barrier for the Pd–Gly monomer mechanism is within 1 kcal/mol of the favored Pd–Ag mechanism. For example, for T_9, computation predicts 62% *meta*-selectivity, and experimental observation affords 63% *meta*-selectivity. When all low-energy conformations for both Pd–Ag and Pd–Gly mechanisms are factored into the Boltzmann distribution to compute combined selectivity, lower *meta*-selectivity is predicted as compared to the Pd–Ag mechanism alone, in accordance with experimental observation. This analysis highlights the need to consider all feasible mechanisms when attempting to predict or rationalize regioselectivities computationally.

Secondary amide template T_7 (entry 7) also provides poor selectivity experimentally. It was determined that for this template the Pd–Gly mechanism is not favorable ($\Delta G^{\ddagger}$ = 27.9 kcal/mol favoring 99% ortho selectivity), but the Pd–Ag mechanism ($\Delta G^{\ddagger}$ = 24.0 kcal/mol) is favored and predicts *meta*-selectivity in 81%. This is inconsistent with the experimental observation of 36% *meta*-selectivity; this inconsistency may be rationalized by the fact that computation predicts that the secondary amide can act as a competing directing group, leading to a higher level of *ortho*-product (see the Supporting Information for a discussion of these transition states).[20] This competing directing group effect of the secondary amide is further supported by the experimental observation that T_8, the *N*-methylated derivative of T_7, affords 86% *meta*-selectivity (Table 1); in the absence of a competitive coordinating group, the nitrile exclusively is responsible for regioselectivity of the products.

2.3. Kinetic Studies on the Influence of Ligand.

As our investigation into the mechanism of *meta*-selective C–H activation of benzoic acids progressed, one major issue emerged: while experimental studies absolutely required MPAA ligand for the reaction to give high yields (Table 2, entry 2), computation suggested MPAA ligand was not involved in the C–H cleavage step as a predominant pathway (instead Pd–Ag dimer is the major pathway).[20] We were curious to determine if the dramatic difference of yield in the presence of ligand (compare 82% with 12%, entries 1 and 2 of Table 2, respectively) was due to improved catalyst lifetime or increased initial reaction rate.[21] Monitoring the reaction by NMR (Supporting Information) over 8 h showed that initial rate could be measured in the first 2 h of the reaction. Using the C–H olefination of the 3-methyl benzoic acid derivative, **2e**, in the presence and absence of *N*-acetyl–glycine, we ran parallel reactions, quenching them at specified intervals, and determined the conversion by ^{1}H NMR spectroscopy of the crude reaction product using a CH_2Br_2 internal standard (Figure 3).

Our experiment deviated slightly from the standard conditions in that 15 mol % $Pd(OAc)_2$ and 30 mol % Ac-Gly-OH ligand were used as it was anticipated that the reaction would be low yielding due to poor turnovers in the ligandless scenario (expected yield after 24 h = 12%). It is evident from the plots in Figure 3 that ligand has a pronounced effect on the initial rate of the reaction: under the present conditions, we observed a 4.25-fold rate increase for reactions with Ac-Gly-OH as compared to those without this ligand (from 3.6

$\times 10^{-3}$ to 1.53×10^{-2} M/min). This finding is in accordance with our previously observed ligand acceleration in the *meta*-C–H olefination of arenes.[21]

Because it was clear from initial rate studies that ligand positively influences the initial rate of *meta*-C–H olefination and this was inconsistent with the preferred computational transition states and to gain more comprehensive mechanistic data, we next sought to determine if C–H cleavage was in fact rate-determining. Thus, the labeled *m*-toluic-d_7 acid-derived template **5** was prepared (see the Supporting Information), and the initial rate of the unlabeled substrate **2e** and the labeled substrate **5** (Figure 4) was measured by performing parallel reactions. The KIE (k_H/k_D) of 1.4 suggests that C–H activation is not turnover limiting.[22] On the other hand, the small but measurable KIE is de facto greater than that of unity and eludes some effect of C–H cleavage on the turnover-limiting step. We next attempted to measure KIE in the ligandless scenario to effectively determine if ligand is involved in the turnover-limiting step. We hypothesized two different scenarios: (A) if the KIE in the absence of ligand matched that in the presence of ligand or if it was equal to unity then ligand is not involved in the turnover-limiting step, and (B) if the KIE in the absence of ligand was dramatically greater than that in the presence of ligand then ligand would necessarily be involved in the turnover-limiting scenario. Upon attempting to carry out further kinetic studies, we noticed that the deuterated substrate **5** did not react in the absence of ligand within 2 h, suggesting a significant KIE, much greater than 1 ($k_H/k_D \gg 1$), but one whose magnitude could not be determined within the error of the NMR measurement (Scheme 1). Overall, these two KIE experiments in tandem suggest that the C–H activation step is either turnover-limiting or at least contributes to the turnover frequency. This information combined with the observed ligand acceleration in Figure 3 suggests that ligand is therefore involved in the turnover-limiting step or at least contributes to turnover frequency.

2.4. Rationalization of Kinetic Data with Further Computation: Development of a Proposed Reaction Coordinate.

Placed in a mechanistic quandary, in which experimental and initial calculations seemed dissonant, we continued computational studies to determine a mechanistic model that accounts for the *meta*-selectivity and enhanced rate in the presence of ligand. While the monomeric palladium glycinate mechanism Pd–Gly would account for the ligand acceleration, it predicts *para*-selectivity ($\Delta\Delta G^{\ddagger}$ = 1.4 kcal/mol) (Table 6). Calculations show that a Pd–Ag heterodimer mechanism is lower in energy and favors the observed *meta*-product ($\Delta\Delta G^{\ddagger}$ = 2.3 kcal/mol). Again, this mechanism does not account for the increased rate in the presence of ligand. Therefore, we investigated the related mechanism Pd–Ag-2 in which one of the acetates of the Pd–Ag heterodimer is replaced by the carboxylate of the *N*-acetyl–glycine (Figure 5). As expected, the barrier and selectivity for this mechanism are unchanged (compare Pd–Ag-2 with Pd–Ag). While mechanism Pd–Ag-2 is feasible, the C–H activation step alone does not account for the kinetic data.

We next considered that the ligand could influence formation of the active catalyst or substrate binding. In the absence of ligand, the most stable heterodimeric catalyst is **7a** (Figure 6), which is 14 kcal/mol less stable than the precatalysts $Pd_3(OAc)_6$ and $Ag_2(OAc)_4$

(the reference state in these calculations). Ligand exchange of the κ^2-acetate with *N*-acetyl–glycine gives the more stable heterodimer **7b**. Other configurations of *N*-acetyl–glycine were studied, but the most stable structure features bidentate coordination to palladium via the imidic acid tautomer of *N*-acetylglycinate, which may act as a hemilabile ligand leading to transition state Pd–Ag-2. Substrate binding and C–H activation steps were next modeled for both active catalysts **7a** and **7b** in a reaction coordinate scheme (Figure 7). The substrate-binding step involves coordination of the nitrile to silver via transition state **8a**/**8b**. Because ligand-binding transition states are notoriously difficult to locate computationally, the barrier for this step was approximated from scans of the potential energy surface. As shown in Figure 7, the MPAA ligand stabilizes the Pd–Ag complexes (**7b** and **9b**) and also lowers the overall barrier for formation of **10b**, the critical intermediate in C–H activation. In the absence of MPAA ligand, the rate-determining step is formation of this intermediate, but the MPAA ligand facilitates formation of **10b**, and the rate-determining transition state becomes C–H activation **11b**. While uncertainty in the energy of transition states **8a** and **8b** must be acknowledged, stabilization of the active Pd–Ag catalyst and acceleration of the substrate-binding step are consistent with the faster reaction in the presence of MPAA ligand.

3. CONCLUSION

We have developed a method for the *meta*-olefination of benzoic acid derivatives by the design and optimization of a unique and curiously flexible template structure. This reaction requires MPAA ligands and silver, which offer dramatic improvements in yield. For simple substrates, yields are very high (>90%) as is *meta*-selectivity (>90%) when Ac-Gly-OH is used. Substitution on the benzoic acid arene ring necessitates the use of different reaction conditions, which still favor *meta*-selectivity but afford the corresponding adducts in moderate-good yields. Computational investigations have elucidated the (A) preferred transition state for C–H activation and (B) conformational requirements of the ideal template structure, one that does not significantly perturb the organization of a Pd–Ag heterodimer. Kinetic studies demonstrated the dependence of initial rate on Ac-Gly-OH, and studies on the KIE coupled with this information undeniably show that C–H activation is turnover-limiting and that Ac-Gly-OH is demonstrably involved in the turnover-limiting step. Finally, we have computed a free energy profile that shows that MPAA stabilizes the Pd–Ag heterodimer prior to C–H activation and lowers the barrier to coordination to the nitrile of the template. Efforts are currently underway in our laboratory to devise similarly flexible and easy-to-make templates analogous to T_3 for *meta*-selective C–H activation of other arene classes, and collaborative efforts between our groups are devoted to the design and implementation of template-approaches for *para*-C–H activation of arenes as well as other remote C–H activation reactions. This study, especially the structural and distortion analyses as well as the dialogue between synthetic and computational chemistry groups, may be used to inspire the development of novel templates for remote C–H activation.

4. METHODS

4.1. Computational Details.

DFT calculations were performed with Gaussian 09.[23] Geometries were optimized with the ωB97X-D functional[24] in the gas phase. A mixed basis set of LANL2DZ(f) for Pd and Ag with 6–31G(d) for all other atoms was used in geometry optimizations. The LANL2DZ basis set was supplemented with an f-type polarization function (exponent 1.472 for Pd, 1.611 for Ag).[25] Thermal corrections were calculated from unscaled vibrational frequencies at the same level of theory using a standard state[26] of 1 mol/L and 343 K. Entropies were corrected for the breakdown of the harmonic oscillator approximation at low frequencies by raising all harmonic frequencies below 100 cm^{-1} to 100 cm^{-1}.[27] Electronic energies were obtained from single-point energy calculations performed with the M06 functional[28] and a mixed basis set of SDD for Pd and Ag with 6–311++G(d,p) for all other atoms. Although the experiments are conducted in hexfluoroisopropanol, this solvent is not available in Gaussian 09. Instead, the SMD[29] solvation model for 2,2,2-trifluoroethanol was used in M06 single-point energy calculations. Computed structures are illustrated using CYLView.[30]

4.2. Experimental Details: General Procedure.

A 5 mL vial equipped with a stir bar was charged with benzoic acid substrate (0.1 mmol), $Pd(OAc)_2$ (0.01 mmol, 10 mol %), Ac-Val-OH (0.02 mmol, 20 mol %), AgOAc (0.3 mmol), and NaOTs (0.1 mmol), olefin of interest (0.25 mmol), and HFIP (1 mL) at room temperature. The vial was capped with a septum insert, stirred vigorously at 70 °C for 24 h, then cooled to room temperature and diluted with EtOAc. The resultant mixture was then filtered through a plug of Celite and further washed with EtOAc. Purification was performed by silica gel-packed flash column chromatography or by preparative TLC using eluents of hexanes/EtOAc or DCM/EtOAc to afford products with the indicated yield.

4.3. Rate and KIE Investigations.

A 5 mL vial equipped with a stir bar was charged with **2e** or **5** (0.1 mmol), $Pd(OAc)_2$ (0.015 mmol, 15 mol %), AgOAc (0.3 mmol), ethyl acrylate (0.25 mmol), and HFIP (1 mL) in both the presence and the absence of ligand Ac-Gly-OH (0.03 mmol, 30 mol %). The vial was capped with a septum insert, stirred vigorously at 70 °C for variable time, then cooled to room temperature, diluted with EtOAc, filtered through a plug of Celite, evaporated, and NMR yields of products of the reaction of **2e** or **5** (**3e** and **6**, respectively) were measured with an internal standard of CH_2Br_2 (0.1 mmol). All points plotted represent the average of two experiments performed separately. Rate constants were determined by multiplication of the slope of the initial rate (occurring in the first 2 h) by molar concentration. Kinetic isotope effect values, reported as k_H/k_D, are reported as the division of the slope of the initial rate for protiated substrate **2e** divided by the slope of the initial rate for deuterated substrate **5**.

Supplementary Material

Refer to Web version on PubMed Central for supplementary material.

ACKNOWLEDGMENTS

We gratefully acknowledge The Scripps Research Institute and the U.S. NSF (CHE-1011898) as well as the NSF Center for Selective C–H Activation (NSF CCHF) for financial support. We thank the NSF and TSRI for financial support of T.G.S.-D. B.L.H.T. gratefully acknowledges the National Institutes of Health for a postdoctoral fellowship (F32GM106596). Computational resources were provided by the UCLA Institute for Digital Research and Education (IDRE) and the Extreme Science and Engineering Discovery Environment (XSEDE), which is supported by the NSF. L.F., S.S.L., and L.H. were supported by the National Natural Science Foundation of China (81172952).

REFERENCES

(1). (a)Giri R; Shi B-F; Engle KM; Maugel N; Yu J-Q Chem. Soc. Rev 2009, 38, 3242. [PubMed: 19847354] (b)Chen X; Engle KM; Wang D-H; Yu J-Q Angew. Chem., Int. Ed 2009, 48, 5094. (c)Wasa M; Engle KM; Yu J-Q Isr. J. Chem 2010, 50, 605. [PubMed: 21552359] (d)Engle KM; Yu J-Q J. Org. Chem 2013, 78, 8927. [PubMed: 23565982]

(2). Engle KM; Mei T-S; Wasa M; Yu J-Q Acc. Chem. Res 2012, 45, 788. [PubMed: 22166158]

(3). (a)Kalyani D; Dick AR; Anani WQ; Sanford MS Tetrahedron 2006, 62, 11483.(b)Godula K; Sames D Science 2006, 312, 67. [PubMed: 16601184]

(4). (a)Hofmann N; Ackermann L J. Am. Chem. Soc 2013, 135, 5877. [PubMed: 23534668] (b)Flemming JP; Berry MB; Brown JM Org. Biomol. Chem 2008, 6, 1215. [PubMed: 18362961] (c)Kakiuchi F; Sekine S; Tanaka Y; Kamatani A; Sonoda M; Chatani N; Murai S Bull. Chem. Soc. Jpn 1995, 68, 62.(d)Satoh T; Miura M Chem. - Eur. J 2010, 16, 11212. [PubMed: 20740508] (e)Guimond N; Gorelsky SI; Fagnou K J. Am. Chem. Soc 2011, 133, 6449. [PubMed: 21452842] (f)Rakshit S; Grohmann C; Besset T; Glorius F J. Am. Chem. Soc 2011, 133, 2350. [PubMed: 21275421] (g)Park SH; Kim JY; Chang S Org. Lett 2011, 13, 2372. [PubMed: 21469713]

(5). (a)Leow D; Li G; Mei T-S; Yu J-Q Nature 2012, 486, 518. [PubMed: 22739317] (b)Dai H-X; Li G; Zhang X-G; Stepan AF; Yu J-Q J. Am. Chem. Soc 2013, 135, 7567. [PubMed: 23614807] (c)Wan L; Dastbaravardeh N; Li G; Yu J-Q J. Am. Chem. Soc 2013, 135, 18056. [PubMed: 24236533]

(6). (a)Lyons TW; Sanford MS Chem. Rev 2010, 110, 1147. [PubMed: 20078038] (b)Daugulis O; Do H-Q; Shabashov D Acc. Chem. Res 2009, 42, 1074. [PubMed: 19552413] (c)Colby DA; Bergman RG; Ellman JA Chem. Rev 2010, 110, 624. [PubMed: 19438203] (d)Wencel-Delord J; Droge T; Liu F; Glorius F Chem. Soc. Rev 2011, 40, 4740. [PubMed: 21666903]

(7). Bag S; Patra T; Modak A; Deb A; Maity S; Dutta U; Dey A; Kancherla R; Maji A; Hazra A; Bera M; Maiti D J. Am. Chem. Soc 2015, 137, 11888. [PubMed: 26361337]

(8). The transition states for C–H activation are cyclophane-like, but do not correspond closely to known cyclophanes. On the basis of atom-count, the *meta*-selective transition state might be considered similar to [5.5]-orthometacyclophane.

(9). (a)Cram DJ; Cram JM Acc. Chem. Res 1971, 4, 204.(b)Bachrach SM J. Phys. Chem. A 2011, 115, 2396. [PubMed: 21351776]

(10). (a)Cheng G-J; Yang Y-F; Liu P; Chen P; Sun T-Y; Li G; Zhang X; Houk KN; Yu J-Q; Wu Y-D J. Am. Chem. Soc 2014, 136, 894. [PubMed: 24410499] (b)Yang Y-F; Cheng G-J; Liu P; Leow D; Sun T-Y; Chen P; Zhang X; Yu J-Q; Wu Y-D; Houk KN J. Am. Chem. Soc 2014, 136, 344. [PubMed: 24313742]

(11). (a)Wang D-H; Mei T-S; Yu J-Q J. Am. Chem. Soc 2008, 130, 17676. [PubMed: 19067651] (b)Zhang Y-H; Shi B-F; Yu J-Q Angew. Chem., Int. Ed 2009, 48, 6097.(c)Chan KSL; Wasa M; Wang X; Yu J-Q Angew. Chem., Int. Ed 2011, 50, 9081.

(12). Li S; Cai L; Ji H; Yang L; Li Gang Nat. Commun 2016, 7, 10443. [PubMed: 26813919]

(13). Zhang Y-H; Shi B-F; Yu J-Q J. Am. Chem. Soc 2009, 131, 5072. [PubMed: 19296661]

(14). Vora HU; Silvestri AP; Engelin CJ; Yu J-Q Angew. Chem., Int. Ed 2014, 53, 2683.

(15). (a)Cong X; Tang H; Wu C; Zeng X Organometallics 2013, 32, 6565.(b)Kubota A; Emmert MH; Sanford MS Org. Lett 2012, 14, 1760. [PubMed: 22409653] (c)Ying C-H; Yan S-B; Duan W-L Org. Lett 2014, 16, 500. [PubMed: 24378012] (d)Pan D; Yu M; Chen W; Jiao N Chem. - Asian J 2010, 5, 1090. [PubMed: 20143374]

(16). Bombrun A Carboline Derivatives. US006043252A, Sep. 16, 1998.

(17). Pfizer I Glucocorticoid receptor modulators. US6380223 B1, Apr. 27, 2000.

(18). Comparison of monomeric, dimeric, and heterodimeric transition states requires calculating the dissociation energies of $Pd_3(OAc)_6$ and $Ag_2(OAc)_4$, which are difficult to calculate accurately. In a previous study (ref 10b), we calculated formation energies of $Pd_2(OAc)_4$ and $PdAg(OAc)_3$, as well as the nitrile-bound versions of these complexes. As compared to more accurate CCSD(T) calculations, M06 consistently underestimated the energy of Pd-homodimers by 5 kcal/mol and that of PdAg-heterodimers by 3 kcal/mol; thus we estimate the error between mechanisms to be in the range of 2–3 kcal/mol.3624243

(19). Interaction energies are −49.2 meta, −46.7 ortho, and −44.2 para.

(20). Anand M; Sunoj RB; Schaefer HF J. Am. Chem. Soc 2014, 136, 5535. [PubMed: 24697273]

(21). Engle KM; Wang D-H; Yu J-Q J. Am. Chem. Soc 2010, 132, 14137. [PubMed: 20853838]

(22). (a)Simmons EM; Hartwig JF Angew. Chem., Int. Ed 2012, 51, 3066.(b)Schramm Y; Takeuchi M; Semba K; Nakao Y; Hartwig JF J. Am. Chem. Soc 2015, 137, 12215. [PubMed: 26334367]

(23). Frisch MJ Gaussian 09, revision C.01; Gaussian, Inc.: Wallingford, CT, 2010.

(24). Chai J-D; Head-Gordon M Phys. Chem. Chem. Phys 2008, 10, 6615. [PubMed: 18989472]

(25). Ehlers AW; Böhme M; Dapprich S; Gobbi A; Höllwarth A; Jonas V; Köhler KF; Stegmann R; Veldkamp A; Frenking G Chem. Phys. Lett 1993, 208, 111.

(26). The correction from 1 atm to 1 mol/L was made by adding $RT\ln(c_s/c_g)$ (i.e., about 2.12 kcal/mol) to the free-energy correction of all structures, where c_s is the standard molar concentration in solution (1 mol/L) and c_g is the standard molar concentration in the gas phase (0.0446 mol/L).sgsg

(27). Ribeiro RF; Marenich AV; Cramer CJ; Truhlar DG J. Phys. Chem. B 2011, 115, 14556. [PubMed: 21875126]

(28). (a)Zhao Y; Truhlar D Theor. Chem. Acc 2008, 120, 215.(b)Zhao Y; Truhlar DG Acc. Chem. Res 2008, 41, 157. [PubMed: 18186612]

(29). Marenich AV; Cramer CJ; Truhlar DG J. Phys. Chem. B 2009, 113, 6378. [PubMed: 19366259]

(30). Legault CYC 1.0b; Université de Sherbrooke: Canada, 2009; http://www.cylview.org.

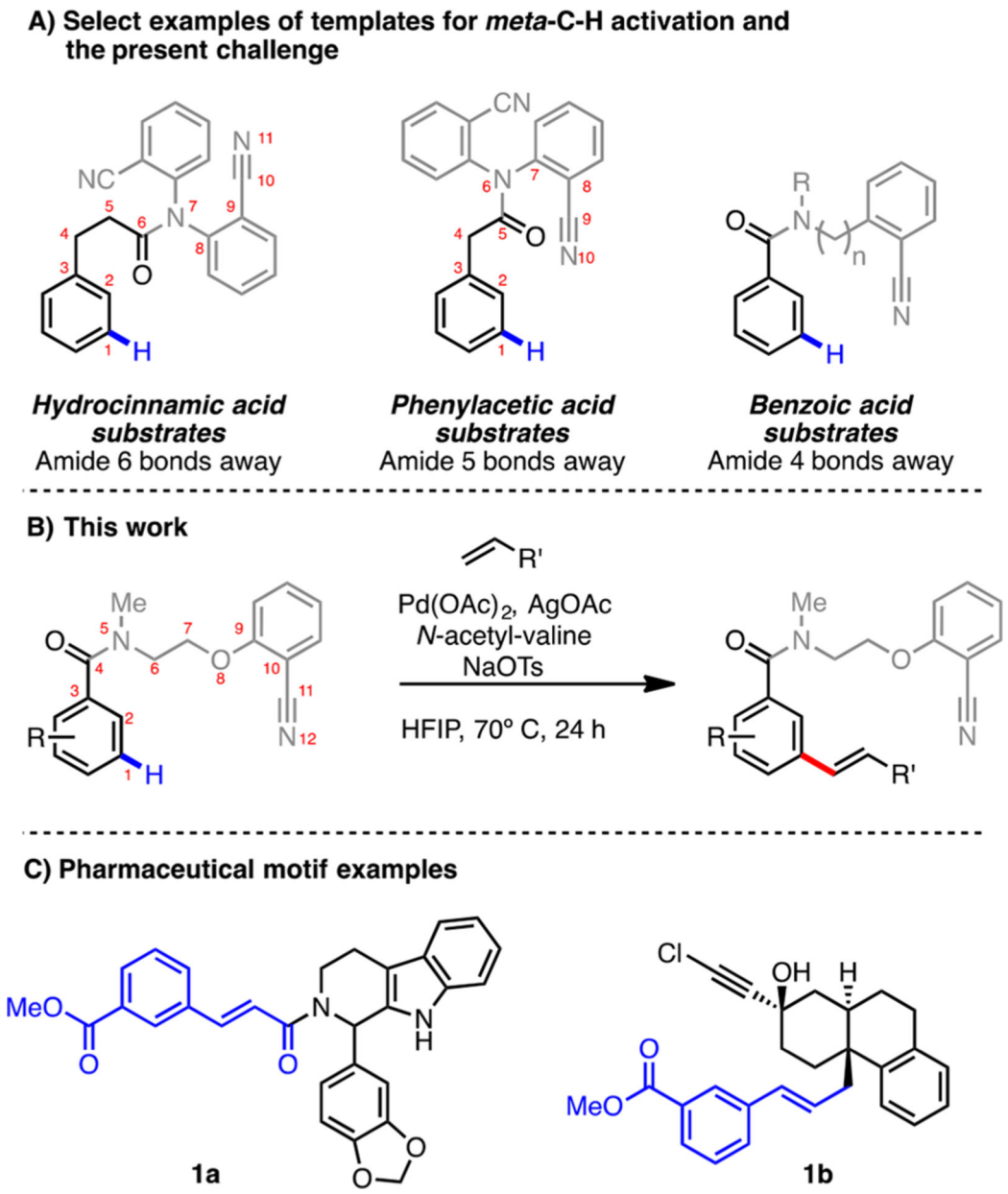

Figure 1.

Palladium-catalyzed *meta*-C–H olefination. (A) Previously disclosed techniques for *meta*-functionalization, (B) the herein detailed method, and (C) pharmaceutical motifs containing the target scaffold of interest.

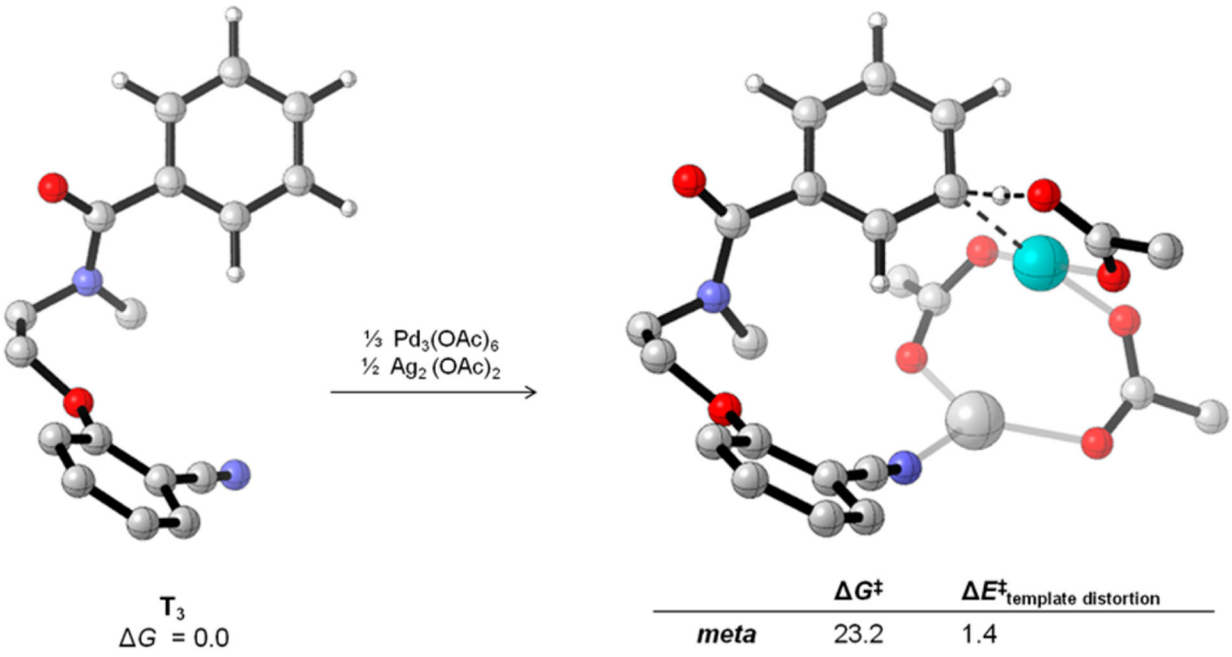

	ΔG‡	ΔE‡template distortion
meta	23.2	1.4
ortho	25.5	3.3
para	30.9	4.8

Figure 2.

Comparison of the lowest energy conformation of template T_3 with the favored transition state.

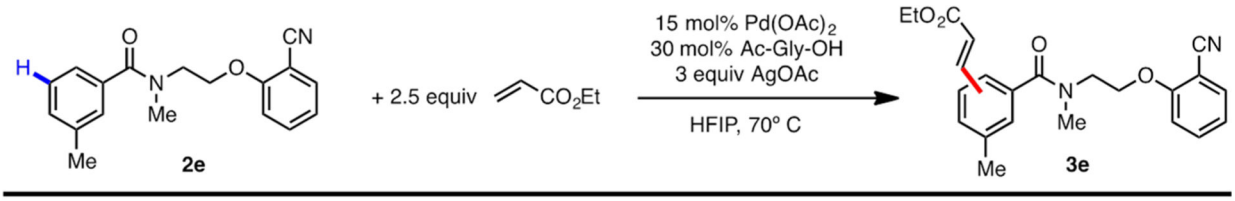

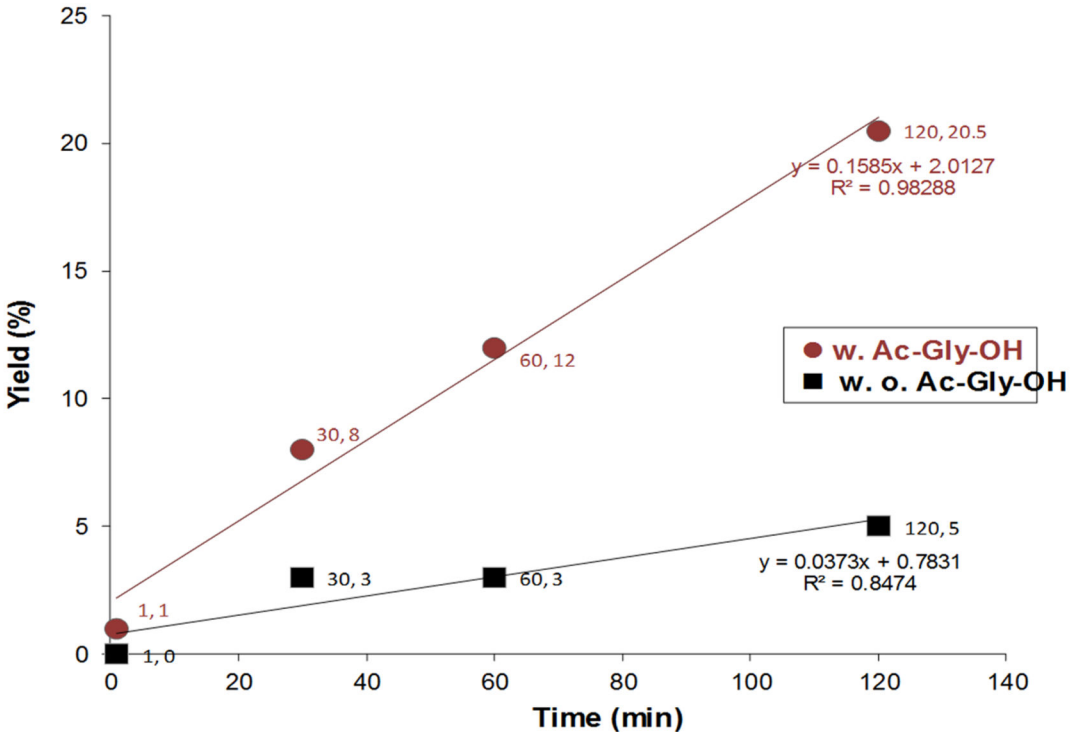

Figure 3.

Rate comparison of *meta*-C–H olefination with and without Ac-Gly-OH ligands. Data points represent the average of two independent trials' NMR yields, calculated using an internal standard of CH_2Br_2 (X, Y = time point, yield). Red ● represent reaction in the presence of Ac-Gly-OH ligand, while ■ represent reaction in the absence of any ligand. Rate comparison was made by dividing initial rate (i.e., slope of the plots). Conditions: 0.1 mmol of substrate, 15 mol % $Pd(OAc)_2$, 30 mol % Ac-Gly-OH, 0.3 equiv of AgOAc, 0.25 equiv of ethyl acrylate, 1 mL of HFIP, 70 °C, variable time.

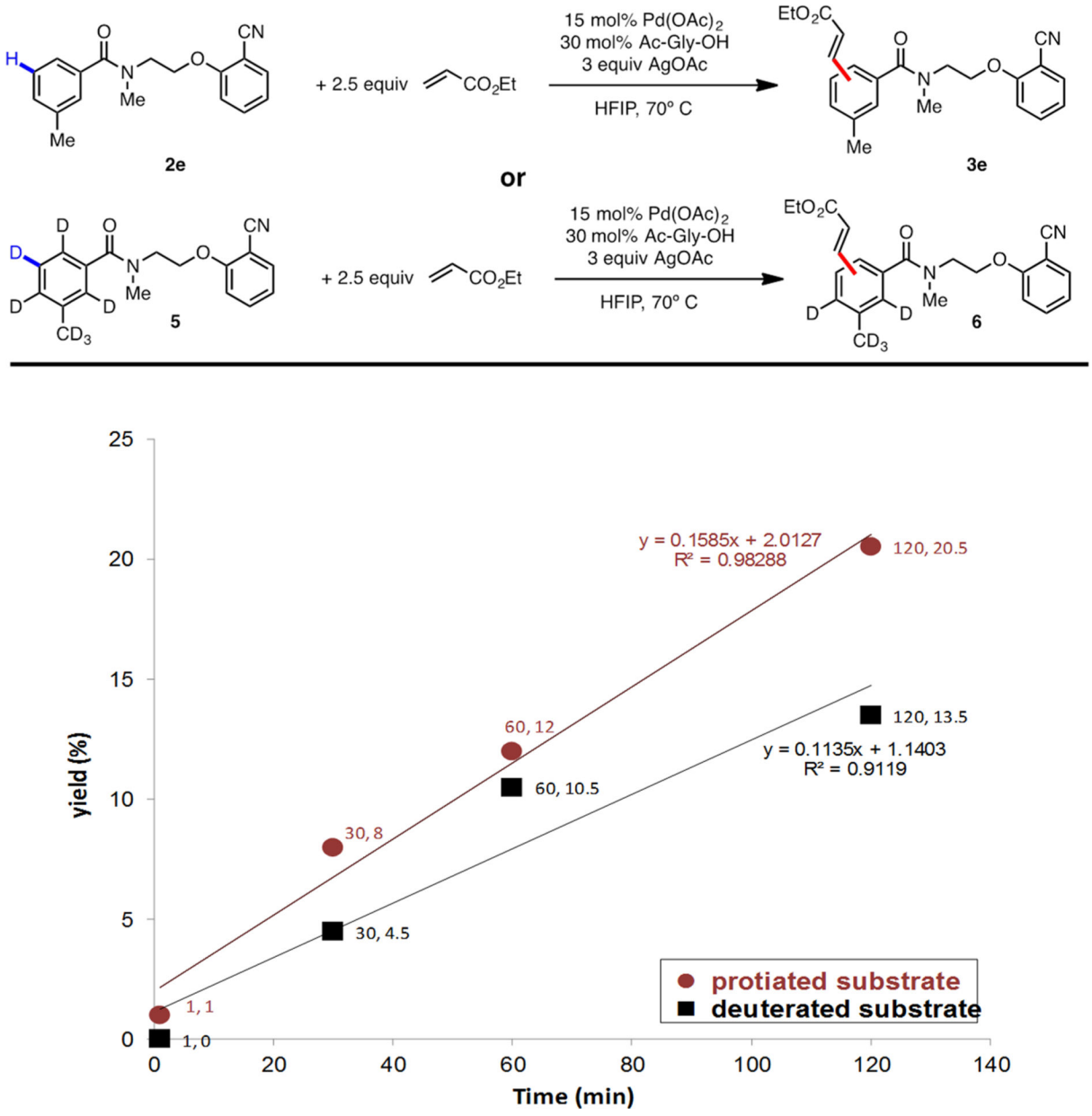

Figure 4.

Kinetic isotope investigations in the presence of MPAA ligand Ac-Gly-OH. Data points represent the average of two independent trials' NMR yields, calculated using an internal standard of CH_2Br_2 (X, Y = time point, yield). Red ● represent protiated substrate, and ■ represent deuterated substrate. Kinetic isotope effect (KIE = k_H/k_D) determined by dividing the slope of the initial rate of the reaction of **2e** by the slope of the initial rate of the reaction of **5**. Conditions: 0.1 mmol of substrate, 15 mol % $Pd(OAc)_2$, 30 mol % Ac-Gly-OH, 0.3 equiv of AgOAc, 0.25 equiv of ethyl acrylate, 1 mL of HFIP, 70 °C, variable time.

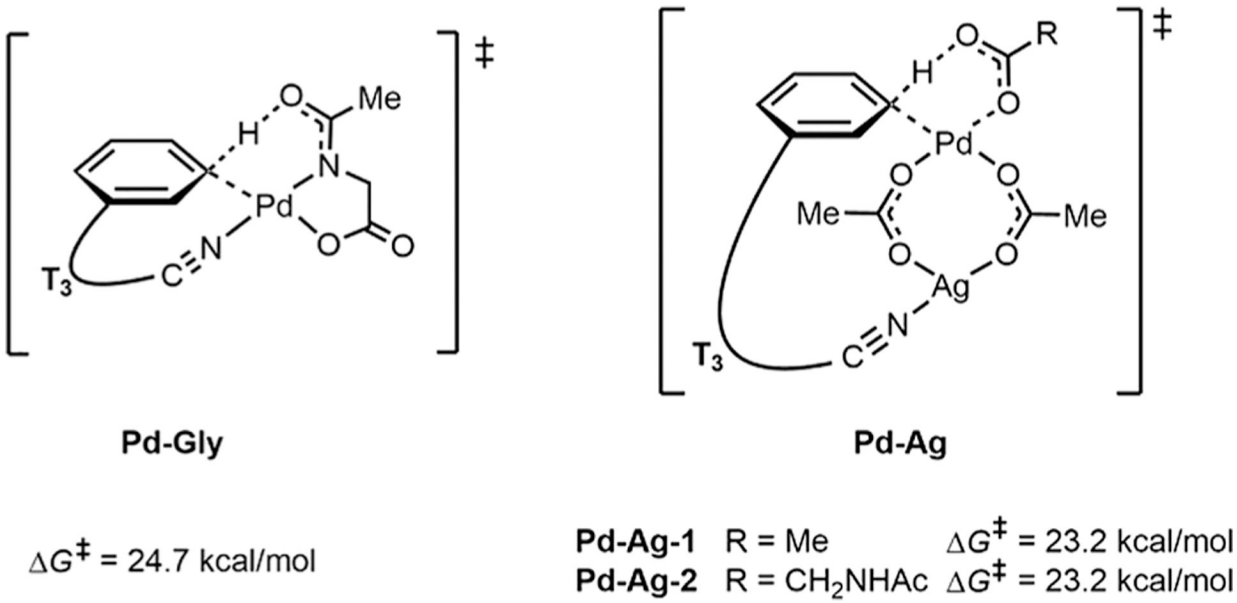

Figure 5.
Transition states Pd–Gly and Pd–Ag for *meta*-C–H activation.

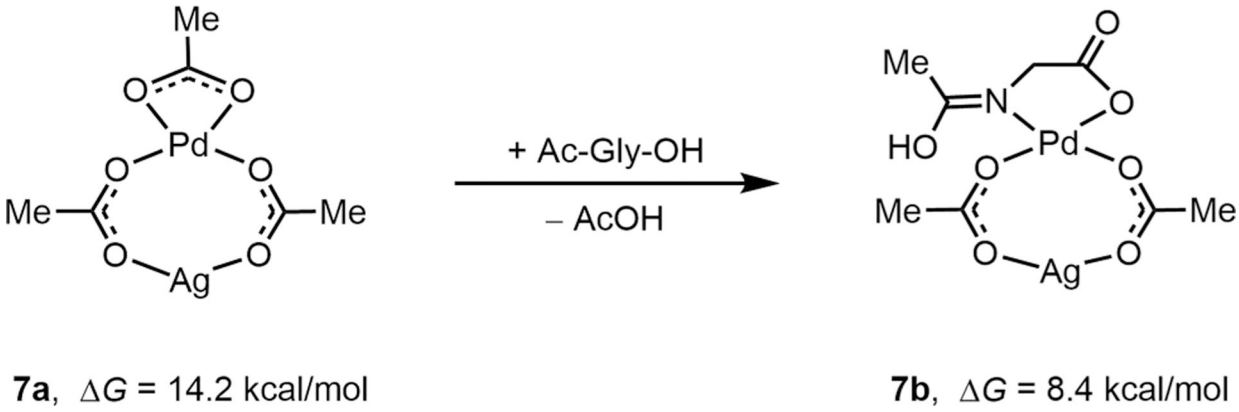

7a, ΔG = 14.2 kcal/mol

7b, ΔG = 8.4 kcal/mol

Figure 6.
Heterodimer catalyst stabilization by *N*-acetyl–glycine.

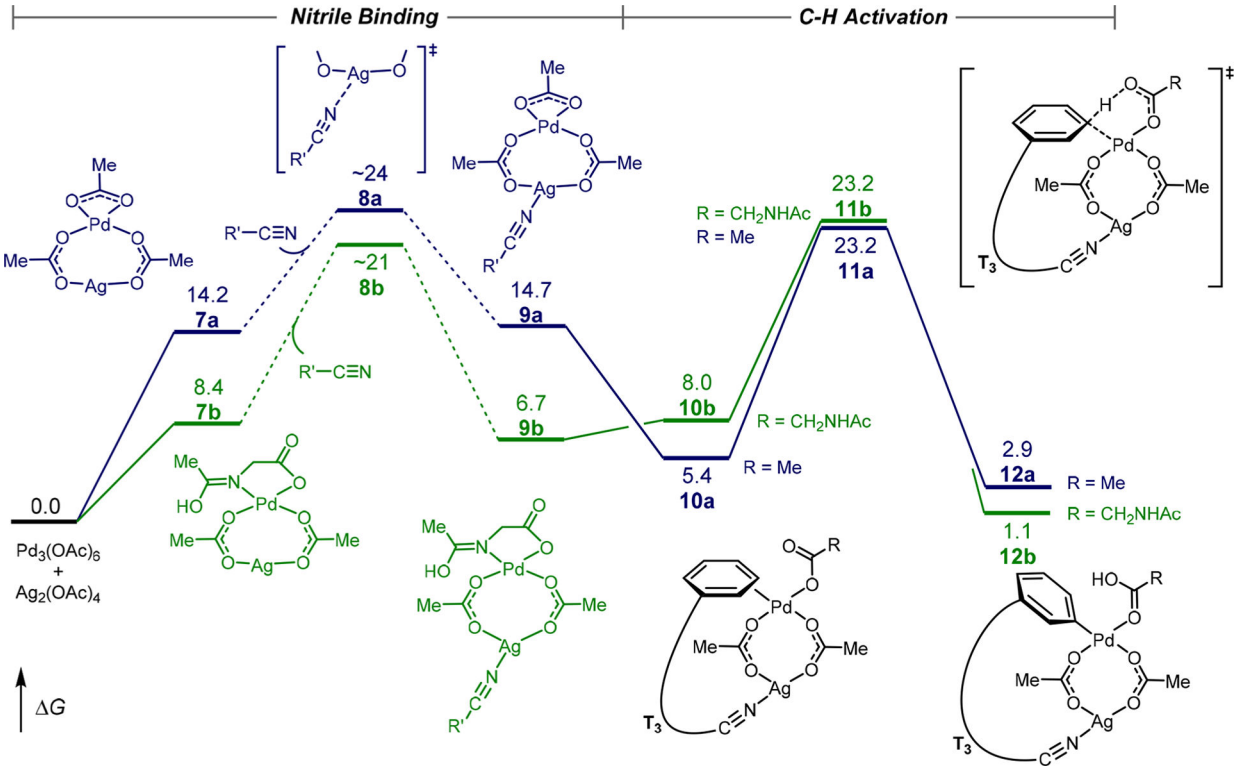

Figure 7.
Free energy profile for substrate binding and C–H activation.

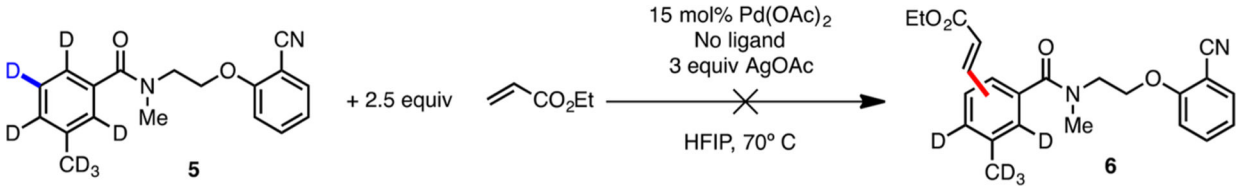

Scheme 1.

Attempted *meta*-Olefination on a Deuterated Benzoic Acid Substrate[a]

[a]Conditions: 0.1 mmol of **5**, 15 mol % $Pd(OAc)_2$, 30 mol % Ac-Gly-OH, 0.3 equiv of AgOAc, 0.25 equiv of ethyl acrylate, 1 mL of HFIP, 70 °C, variable time.

Table 1.

J Am Chem Soc. Author manuscript; available in PMC 2024 May 11.

Initial Templates Designed and Evaluated for Pd(II)-Catalyzed C–H Olefination[b]

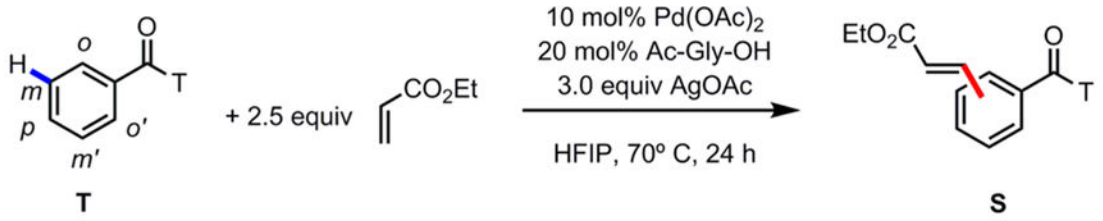

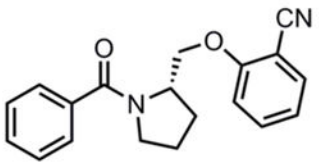

T1: 76%
m:others = 88:12
mono:di = 5:1

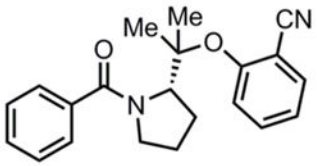

T2: 43%
m:others =95:5
mono:di = 13:1

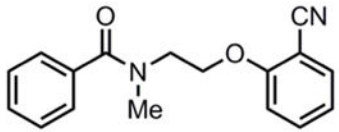

T3: 98%
m:others =91:9
mono:di = 10:1

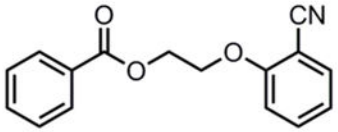

T4: 56%[a]
m:others = 47:53

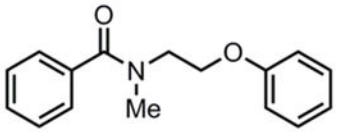

T5: 49%[a]
m:others = 48:52

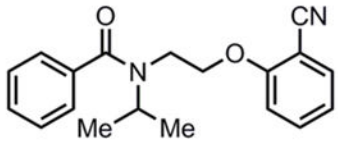

T6: 72%
m:others =76:24
mono:di = 2.5:1

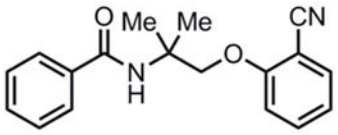

T7: 26%
m:others =36:64
mono:di = 10:1

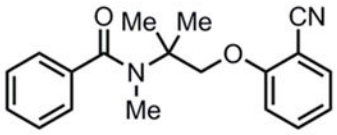

T8: 66%
m:others = 86:14
mono:di =7.2:1

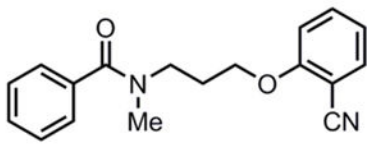

T9: 16%
m:others = 63:37
mono:di = 10:1

[a] Only monomeric olefination adduct observed.

[b] Conditions: 0.1 mmol of T, 10 mol % $Pd(OAc)_2$, 20 mol % Ac-Gly-OH, 0.25 mmol of ethyl acrylate, 1 mL of HFIP, 70 °C, 24 h. Yields and selectivity determined by NMR with an internal standard of CH_2Br_2.

Table 2.

Screening Variables in the Reaction of a Simple Benzoic Acid Derivative[a,b]

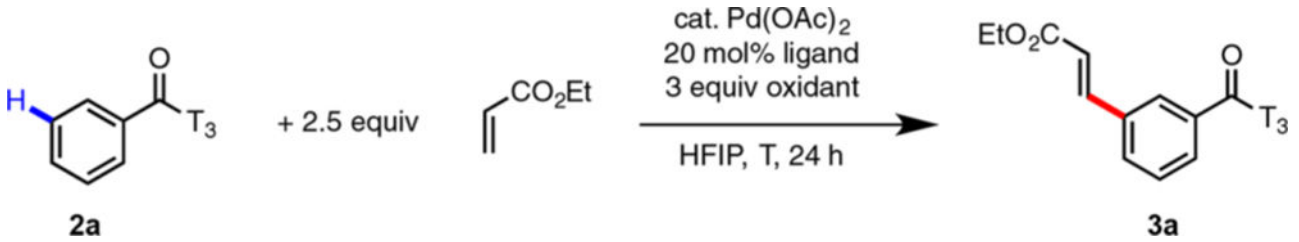

2a **3a**

entry	ligand (20 mol %)	Ooxidant	$Pd(OAc)_2$	*T* (°C)	yield (%)	meta/others	mono/di
1	Ac-Gly-OH	AgOAc	10%	70	82	95/5	8.2/1
2		AgOAc	10%	70	12	93/7	7.0/1
3	Ac-Gly-OH		10%	70	44	90/10	10.0/1
4	Ac-Gly-OH	AgOAc	5%	70	70	90/10	5.3/1
5	Ac-Gly-OH	AgOAc	10%	60	98	91/9	11.3/1
6	Ac-Gly-OH	AgOAc	10%	50	68	91/9	7.6/1
7	Ac-Gly-OH	AgOAc	10%	40	54	93/7	2.6/1
8	Ac-Gly-OH	AaOAc	10%	rt	21	96/4	2.6/1

[a] Conditions: 0.1 mmol of substrate, 0.25 mmol of ethyl acrylate, 0.005 or 0.01 mmol of $Pd(OAc)_2$, 0.02 mmol of Ag-Gly-OH, 0.3 mmol of AgOAc, 1 mL of HFIP, 70 °C for 24 h.

[b] Selectivity refers to the ratio of meta:others of monoolefinated products, as determined by crude ^{1}H NMR spectroscopy.

Table 3.

Optimization of Reaction for Substituted Benzoic Acids[a,b]

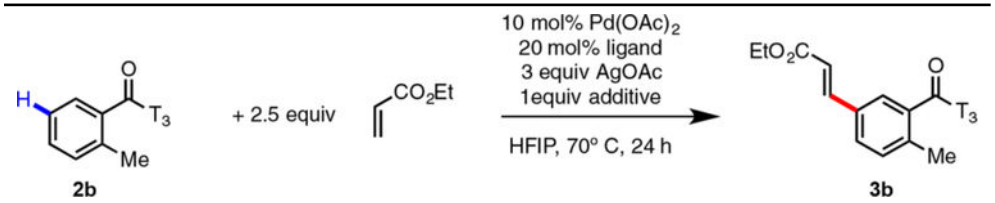

entry	ligand (20 mol %)	additive (1 equiv)	yield (%)	meta/others
1	Ac-Gly-OH		42	60/40
2	Ac-Gly-OH	NaH_2PO_4	24	61/39
3	Ac-Gly-OH	NaH_2PO_4	4	33/67
4	Ac-Gly-OH	Na_3PO_4	9	33/67
5	Ac-Gly-OH	$khco_3$	23	45/55
6	Ac-Gly-OH	K_2CO_3	12	31/69
7	Ac-Gly-OH	NaOAc	11	31/69
8	Ac-Gly-OH	NaOTs	43	60/40
9	Ac-Gly-OH	LiOAc	18	40/60
10	Fmoc-Gly-OH		1	10/90
11	Fmoc-*t*-Bu-Gly-OH		15	50/50
12	Boc-Ph-Gly-OH		0	
13	Boc-cyclohexyl-Gly-OH		trace	
14	*N*-chloroacetyl-Gly-OH		8	30/70
15	Trt-Gly-OH		0	
16	*N*,*N*-dimethyl-Gly-OH		0	
17	Ac-Ala-OH		53	62/38
18	Ac-Leu-OH		59	67/33
19	Ac-t-Leu-OH		38	71/39
20	Ac-Val-OH		63	78/32
21	Ac-Val-OH	*p*-TsOH	43	47/53
22	Ac-Val-OH	CF_3CO_2H	35	38/62

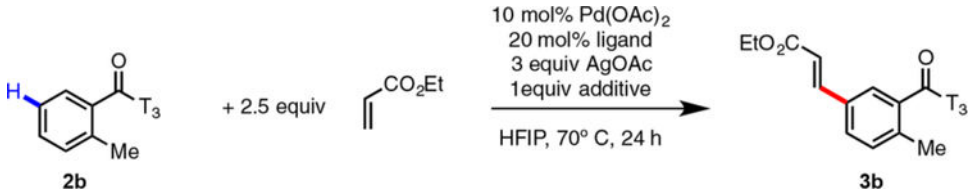

entry	ligand (20 mol %)	additive (1 equiv)	yield (%)	meta/others
1	Ac-Gly-OH		42	60/40
23	Ac-Val-OH	NaOTs	91	95/5

[a] Conditions: 0.1 mmol of substrate, 0.25 mmol of ethyl acrylate, 0.01 mmol of $Pd(OAc)_2$, 0.02 mmol of ligand, 0.3 mmol of AgOAc, 0.1 mmol of additive, 1 mL of HFIP, 70 °C for 24 h.

[b] Selectivity refers to the ratio of meta:others of monoolefinated products, as determined by crude ^1H NMR spectroscopy.

Table 4.

Substrate Scope of the *meta*-Olefination of Benzoic Acids[a,b]

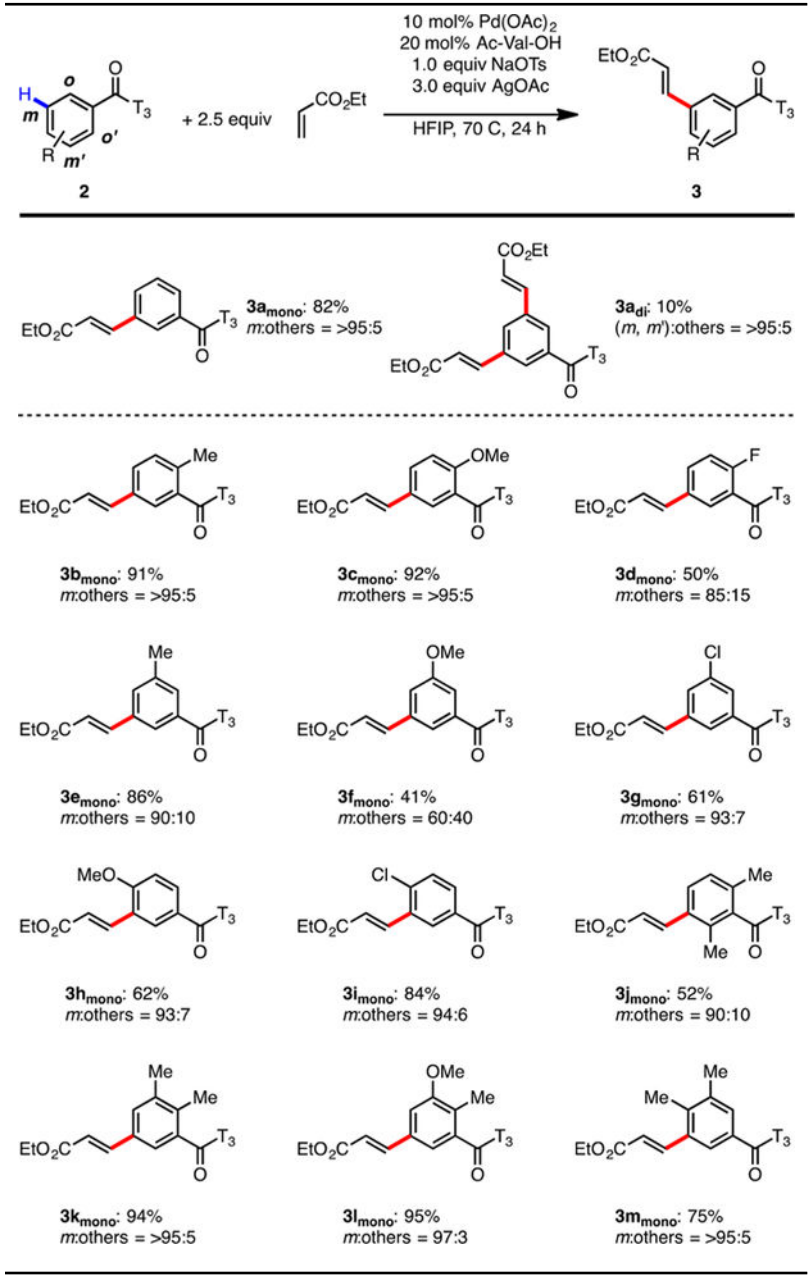

J Am Chem Soc. Author manuscript; available in PMC 2024 May 11.

[a] Conditions: 0.1 mmol of substrate, 0.25 mmol of ethyl acrylate, 0.01 mmol of $Pd(OAc)_2$, 0.02 mmol of Ac-Val-OH, 0.3 mmol of AgOAc, 0.1 mmol of NaOTS, 1 mL of HFIP, 70 °C for 24 h.

[b] Selectivity refers to the ratio of meta:others of monoolefinated products, as determined by crude ^1H NMR spectroscopy.

Table 5.

Olefin Scope of the *meta*-Olefination of Benzoic Acids[a,b]

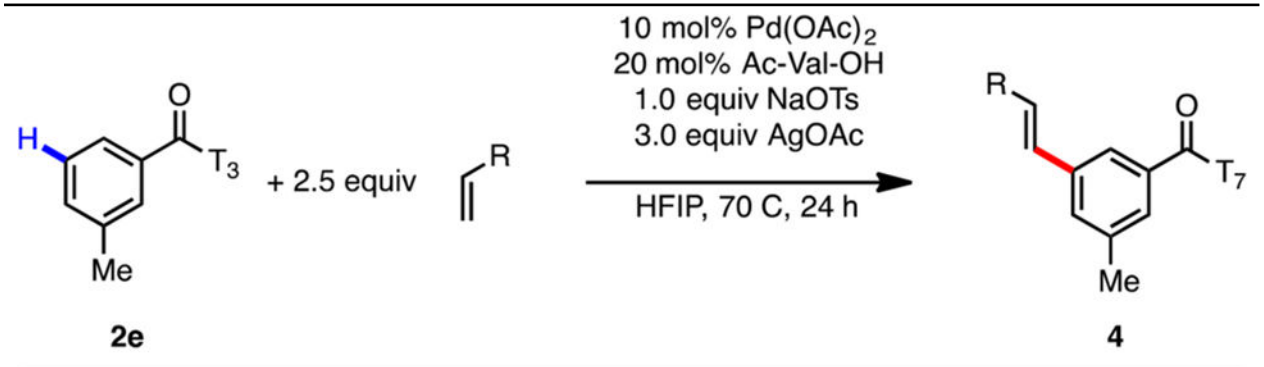

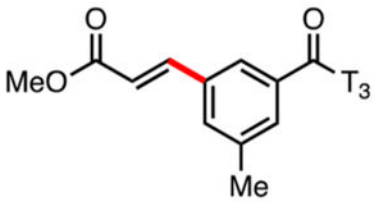

4a: 86%
m:others>95:5

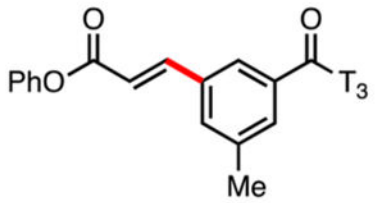

4b: 89%
m:others>95:5

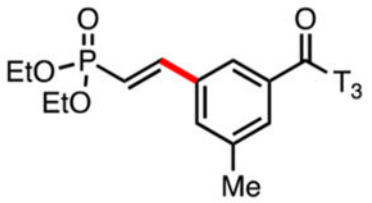

4c: 92%
m:others>95:5

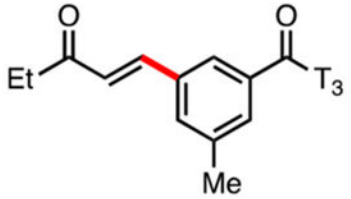

4d: 84%
m:others>95:5

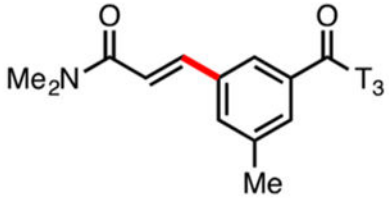

4e: 72%
m:others =70:30

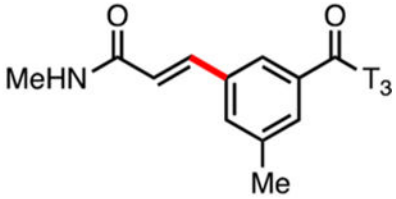

4f: 68%
m:others = 78:22

[a] Conditions: 0.1 mmol of substrate, 0.25 mmol of olefin, 0.01 mmol of $Pd(OAc)_2$, 0.02 mmol of Ag-Val-OH, 0.3 mmol of AgOAc, 0.1 mmol of NaOTs, 1 mL of HFIP, 70 °C for 24 h.

[b] Selectivity refers to the ratio of meta:others of monoolefinated products, as determined by crude ^1H NMR spectroscopy; yields were calculated using an internal standard for CH_2Br_2.

Table 6.

C–H Activation Transition States for Optimal Template T_3[a]

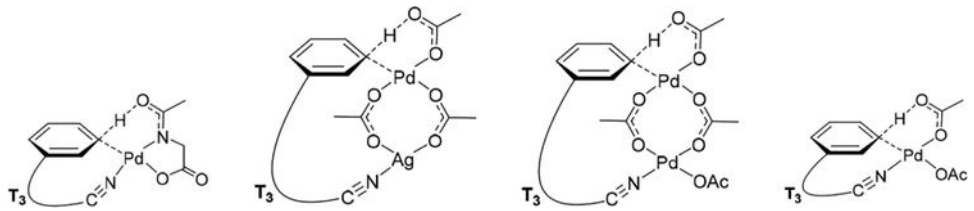

	Pd-Gly	Pd-Ag	Pd-Pd	Pd
$\Delta G^{\ddagger}$, *meta*	26.1	**23.2**	**26.2**	33.1
$\Delta G^{\ddagger}$, *ortho*	28.7	25.5	30.0	33.1
$\Delta G^{\ddagger}$, *para*	**24.7**	30.9	38.0	**30.3**
computed selectivity	13:0:87 *m:o:p*	98:2:0 *m:o:p*		
combined selectivity	94:2:4 *m.o.p*			

[a]Note that artistic rendering of the template structure has been simplified.

J Am Chem Soc. Author manuscript; available in PMC 2024 May 11.

Table 7.

Comparison of Computed and Experimental Regioselectivity of Template Derivatives

Entry	Template	Pd-Gly Mechanism $\Delta G^{\ddagger}$ (kcal/mol) *Selectivity*	Pd-Ag Mechanism $\Delta G^{\ddagger}$ (kcal/mol) *Selectivity*	Combined Selectivity (*meta*:others)	Experimental Selectivity (*meta*:others)
1	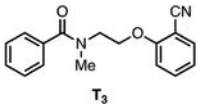 T_3	24.7 87% *para*	23.2 98% *meta*	94:6	91:9
2	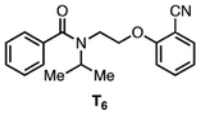 T_6	27.0 60% *meta*	22.6 92% *meta*	91:9	76:24
3	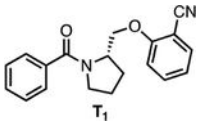 T_1	26.5 76% *para*	24.1 99% *meta*	96:4	88:12
4	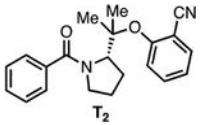 T_2	24.5 89% *meta*	22.8 85% *meta*	85:15	95:5
5	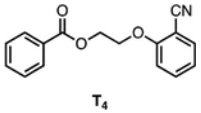 T_4	24.5 91% *ortho*	23.9 85% *meta*	69:31	47:53
6	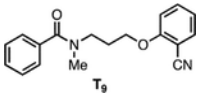 T_9	26.2 99% *para*	25.3 71 % *meta*	62:38	63:37
7	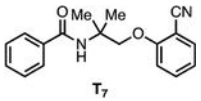 T_7	27.9 99% *ortho*	24.0 81% *meta*	81:19	36:64